Sensors & Actuators: A. Physical 358 (2023) 114448

Contents lists available at ScienceDirect

Sensors and Actuators: A. Physical

journal homepage: www.journals.elsevier.com/sensors-and-actuators-a-physical

Ultrasensitive flexible strain sensors based on graphene nanoplatelets doped poly(ethylene glycol) diglycidyl ether: Mask breathing monitoring for the Internet of Things

Antonio del Bosque [a,*], Xoan F. Sánchez–Romate [a], David Patrizi [b,c], José Sánchez del Río Sáez [b,c], De-Yi Wang [b,d,**], María Sánchez [a], Alejandro Ureña [a,*]

[a] Materials Science and Engineering Area, Escuela Superior de Ciencias Experimentales y Tecnología, Universidad Rey Juan Carlos, Calle Tulipán s/n, 28933 Móstoles, Madrid, Spain

[b] IMDEA Materials Institute, Calle Eric Kandel 2, 28906 Getafe, Madrid, Spain

[c] Departamento de Ingeniería Eléctrica, Electrónica Automática y Física Aplicada, ETSIDI, Universidad Politécnica de Madrid, Ronda de Valencia 3, 28012 Madrid, Spain

[d] Universidad Francisco de Vitoria, Carretera Pozuelo, Majadahonda Km 1, 800, 28223 Pozuelo de Alarcón, Madrid, Spain

ARTICLE INFO

Keywords:
Graphene nanoplatelet
Strain sensor
Internet of Things
Breathing monitoring

ABSTRACT

Ultrasensitive and stretchable strain sensors based on graphene nanoplatelet (GNP) doped poly(ethylene glycol) diglycidyl ether (PEGDGE) for human motion monitoring purposes with remote tracking by using Internet of Things (IoT) technologies are synthesized. The quasi–static and cycling responses under both tensile and compression conditions of nanocomposites are studied in detail. On one hand, quasi-static analysis shows very high values of the gauge factor, reaching values around 50–100 at low strain levels (1–2%) and 1000–2500 at high strain levels (10%) in tensile mode, with increasing sensitivity with decreasing GNP content. In addition, electromechanical response under 500 tensile and compression load cycles up to 1%, 2.5%, and 5% strain levels proves their high stability and as a result, their high sensitivity to detect a low degree of strain levels. Three general proofs–of–concept demonstrate that these sensors can detect several types of deformations such as pressure, bending, and twisting. Finally, human breathing is monitored with the sensor attached to a conventional mask. Different breath rhythms combining the calm and excited states of a person walking are remotely sent and monitored on the internet by using different IoT platforms.

1. Introduction

Nowadays, there is an increasing interest in the development of novel inspection techniques and wearable sensors for health monitoring technologies. There are many sensing methods, for example, those based on ultrasonic, guided waves, fiber Bragg, or acoustic emission technologies [1–3]. However, they make use of complex mathematical and statistical tools and do not give information enough about the health of the asset [4,5], evermore when it is sent remotely. For this reason, other materials-based techniques with more sophisticated communication protocols are demanded.

As an alternative to these traditional techniques, the development of reinforced polymers with conductive nanoparticles is proposed. The basis of this type of material for sensing applications is that these conductive nanoparticles promote the creation of conducting networks inside the insulating polymer [6] once a critical volume fraction is reached, called the percolation threshold. When the nanocomposite is either stretched or compressed, the electrical resistance of the conductive network changes as a function of the applied mechanical strain. Electrical resistance variations beyond these stretching/compressing levels are caused by geometrical changes in their structure, the intrinsic resistive response of active materials, the tunneling effect, or disconnection mechanisms [7–9]. After releasing the nanocomposite from strain, the resistance reversibly recovers to its initial values. Thus, the deformation state can be studied by analyzing the change in the electrical resistance which is the principle that governs resistive strain

* Corresponding authors.
** Corresponding author at: IMDEA Materials Institute, Calle Eric Kandel 2, 28906 Getafe, Madrid, Spain.
E-mail addresses: antonio.delbosque@urjc.es (A. del Bosque), deyi.wang@imdea.org (D.-Y. Wang), alejandro.urena@urjc.es (A. Ureña).

https://doi.org/10.1016/j.sna.2023.114448
Received 14 April 2023; Received in revised form 18 May 2023; Accepted 19 May 2023
Available online 22 May 2023

sensors.

Graphene nanoplatelets (GNPs) are one of the types of carbon nanoparticles that provide higher sensitivity to nanocomposite–based sensors, especially when compared to carbon nanotubes (CNT), carbon black (CB) or carbon nanofibers (CNF) [10–12]. This fact can be explained due to the 2D nature of GNPs, where the tunneling effect mechanisms are much more accused concerning the other carbon nanoparticles mentioned because of their higher tunneling area. Regardless of the type of stretchable strain sensors, GNPs have been incorporated into stretchable supporting materials such as silicone elastomers (PDMS or Ecoflex) [13,14], rubbers [15,16], thermoplastic [17], and medical adhesive films [18]. Moreover, natural fiber–based materials such as wool, wood, or flax have been widely used as supporting substrates for the manufacture of strain sensors [19]. As can be deduced from the state of the art, different types of thermoplastic and elastomers have been used as matrices for flexible sensors, however, other materials have not yet been explored in detail, such as flexible epoxy resins.

In recent years, strain sensor based on GNP/PDMS has been widely reported to provide a stretchability of up to 65% with a high gauge factor [20,21]. Another strategy is to develop porous structured GNP strain sensors because they have a low percolation threshold (2–4 wt%) [22–25]. Moreover, three–dimensional graphene foam has been reported before for high–performance strain sensors, however, some problems such as high–cost preparation, low sensitivity, and low stretchability remain [26]. In all these works, the potential these materials have in sense is evident, although the development of a full–characterized wearable strain sensor for smart devices has not been reported yet.

The Internet of Things (IoT) in Health Monitoring has recently irrupted very strongly in the biomedical sensing field [27–29]. The relevance that monitoring vital parameters such as body temperature, lungs capacity, and environmental humidity, breathing and heart rhythms, chemical agents in gaseous or liquid states, etc. have nowadays is increasing and plays an important role in therapy and illness diagnosis, also during pandemic outbreaks such as the last one of COVID in 2019 [30]. An application that sends remotely patients vital constants such as breathing and heart rhythm and that allows monitoring his/her health state with a deep impact in today's healthcare sensing field is the smart face mask [31], which is a–located face mask with different sensors integrated. It often operates online monitoring via the internet of multiple biological parameters such as CO_2 concentration, breath expiration temperature, cardiac pulse, breath rhythm, amount of air intake, etc., and environmental variables such as humidity, barometric pressure, pollution, and environmental temperature.

As reported in the literature [32,33], information from different sensors is remotely sent to several nodes constituting broad sensing networks. These networks can resend previous parameters to central units connected to IoT platforms so that vital constants of patients can be visualized on the internet. In addition, different wireless communication technologies such as WiFi, SigFox LoRaWAN, Narrow Band, LTE–M, Cellular, etc. [34–36] can be used for sending the information remotely. Furthermore, each protocol presents very low energy consumption and different connectivity characteristics such as different amounts of information sent, time of flight of the packages, and distance range. In this work, LoRa sensors and LoRaWAN were chosen to send the information remotely to a gateway because of their excellent characteristics in terms of long–range distance and open connectivity, covering communications range up to 20 km between emitters and receivers in interurban areas and hundreds of kilometers in places where there is no electromagnetic interference such as in open air and in the outer space.

For these reasons, this work is focused on the development of a highly stretchable and easily–scalable strain sensor made of a flexible epoxy resin poly(ethylene glycol) diglycidyl ether (PEGDGE) reinforced with GNPs. The electromechanical analysis, in terms of quasi–static and cycling response, allowed determining the sensitivity and the repeatability of the electrical resistance response under different values of applied strain. Moreover, the electromechanical response was carried out under tensile and compression conditions to get a deeper knowledge of their strain monitoring capabilities. Finally, several operational demonstrations were also carried out with the optimized sensor, highlighting the never–before–seen proof of concept with a GNP/PEGDGE sensor attached to the surface of the mask. This sensor was connected to a LoRa wireless emitter which allowed monitoring of the subject's breathing rhythm under different physical conditions (relaxed, stressed, and walking) in The Things of Stack (TTS) IoT platform in real time.

2. Materials and methods

2.1. Materials

Strain sensors were manufactured with GNPs dispersed in a PEGDGE resin. GNPs were purchased from XG–Science with a commercial name M25. They have a thickness of 6–10 nm with an average lateral size of 25 μm, and an electrical conductivity of $\sim 10^7$ S/m parallel to the surface and $\sim 10^2$ S/m in the transversal direction.

The matrix was a flexible epoxy resin formed by poly(ethylene glycol) diglycidyl ether (PEGDGE) with 4,4–diaminodiphenylsulfone (DDS) as a hardener. PEGDGE has a viscosity of 60–110 mPa·s at 25 ºC with a molecular weight of 500 g/mol, and its flexibility is due to the existence of 8–9 EO groups in its structure. Both reagents were purchased from SigmaAldrich.

2.2. Manufacturing of GNP/PEGDGE nanocomposites

Nanocomposites were manufactured with 2, 4, 6, 8, and 10 wt% GNPs to determine the percolation threshold of the GNP/PEGDGE system, that is, the lower GNP content that makes it electrically conductive. Fig. 1a shows the schematic diagram of the nanocomposites manufacturing process. In this regard, GNPs were dispersed by three roll milling process using an EXAKT 80E machine. This method causes the disaggregation of GNP agglomerates when the mixture passes between the gaps of the three consecutive rolls rotating at different speed ratios of 1:3:9, being 250 rpm the rotating speed of the last roll. The parameters of the three–roll milling process were optimized in a previous study [37] and they consisted of a unique cycle because it was proved that by increasing the number of cycles, damage to the GNPs was produced. Specifically, breakage or downsizing of the GNPs occurs due to the high shear forces involved and their low flexural strength.

After the dispersion phase, a degassing step of the mixture was carried out at 100 ºC for 20 min under vacuum conditions by magnetic stirring. The high temperature promotes the decrease in the viscosity of the sample, which facilitates the evacuation of the trapped air, together with the magnetic agitation and the vacuum pressure. Then, DDS was added to the mixture in a 100:25 ratio (monomer:hardener in its stoichiometric ratio) and mixed manually for 2 min. Finally, the mixture was placed in a metallic mold with the shape of the final probes which had been previously smeared with a layer of release agent based on polyvinyl alcohol (Castro Composites). Probes were cured in an oven at 160 ºC for 5 h, as it was optimized in previous work [11].

2.3. Microstructural characterization

Nanocomposites were fractured under cryogenic conditions to analyze the dispersion state achieved in the GNP/PEGDGE samples. The fracture surfaces were coated with a thin layer of gold with the sputtering technique, and they were observed by Scanning Electron Microscopy (SEM) with the Hitachi S3400N Microscope.

2.4. Electrical conductivity measurement

The electrical conductivity of the nanocomposites was measured

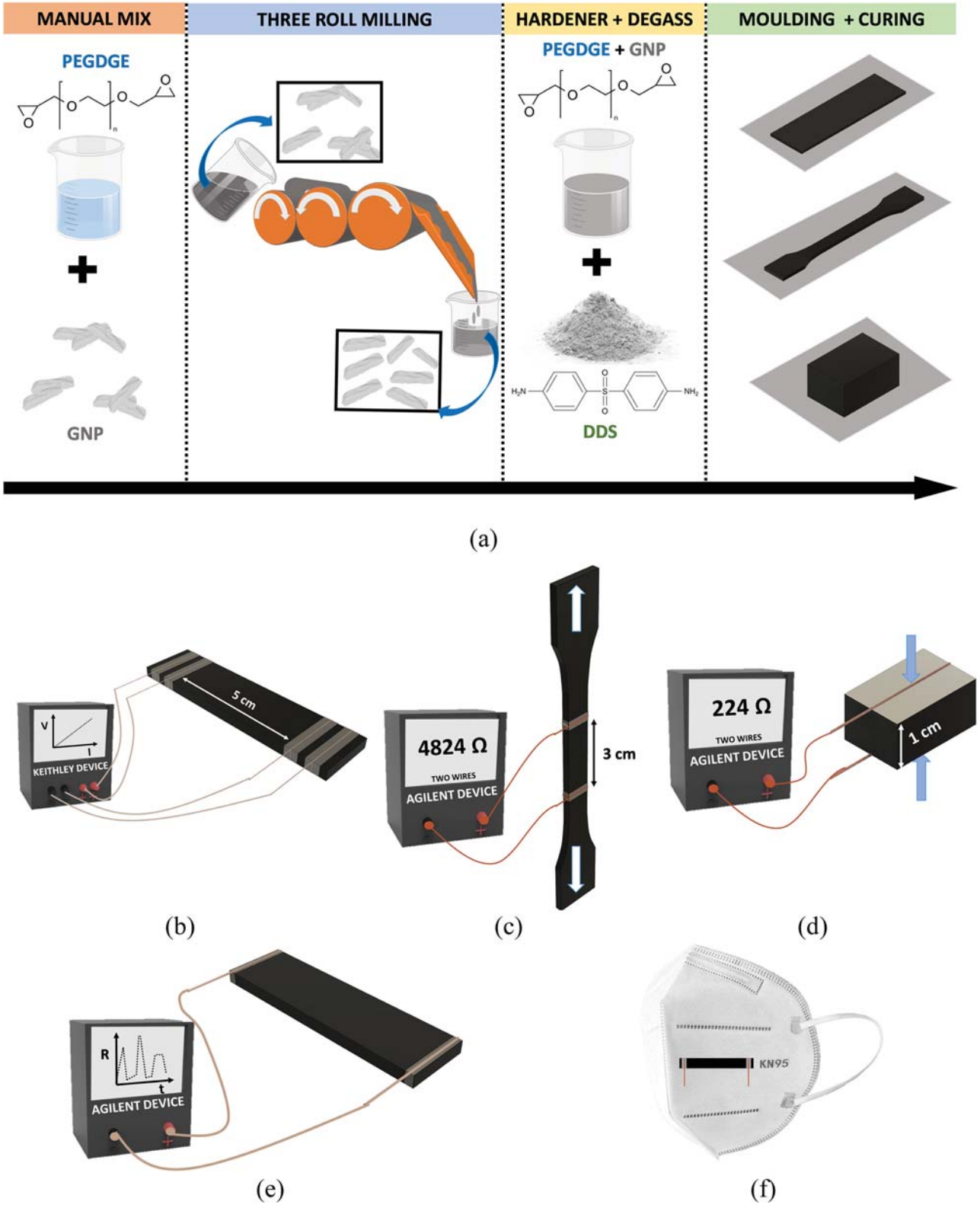

Fig. 1. : (a) Schematic diagram of the GNP/PEGDGE nanocomposites manufacturing process. Schematics of samples/measurements and electrodes' disposition in (b) electrical conductivity measurements, (c) tensile and (d) compression tests for strain monitoring characterization, (e) proof–of–concept sensor and (f) FFP2 mask for human breath monitoring. (g) Experimental set–up of the electronics and LoRa communication system used for human breathing monitoring with the GNP/PEGDGE strain sensor.

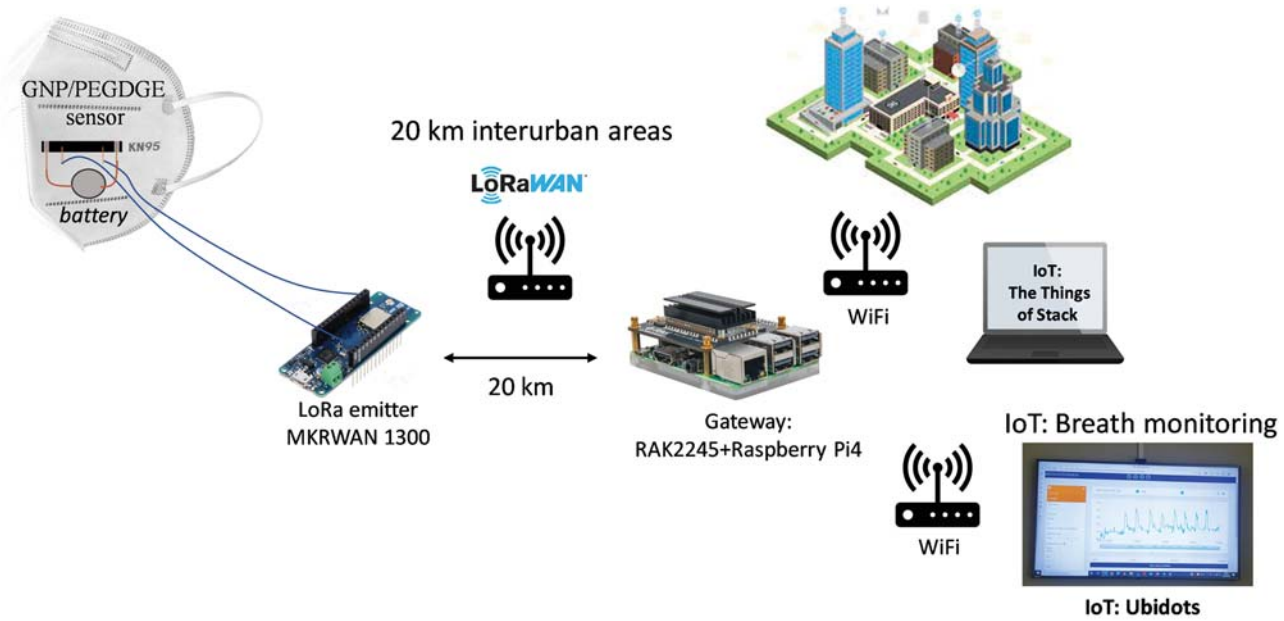

Fig. 1. (*continued*).

using a Keithley 2450 Source Meter Unit instrument. It was determined by applying different values of voltage and recording the current with the four–probe measurement. Following the Ohm Law, the electrical resistance was calculated from the slope of the current–voltage curve at 0–100 V for low conductivity and 0–10 V for high conductivity nanocomposites (that are 8 and 10 wt% GNP). Three electrical conductivity specimens with $60 \times 20 \times 3\ mm^3$ dimensions (50 mm between the closest contacts) were tested for each condition. For these experiments, four copper electrodes were attached to the sample surface by gluing them with conductive silver ink to minimize the contact resistance (see Fig. 1b).

2.5. Strain sensing tests

The variation of electrical resistance of GNP/PEGDGE nanocomposites was recorded using a digital multimeter Agilent 34465 A during tensile and compression tests. Three tensile and compression samples of 8 and 10 wt% GNP were tested in a universal testing machine Zwick Z100 with a load cell of 500 N.

Firstly, tensile specimens were tested according to ISO 527–1:2019 with a crosshead speed of 10 mm/min and a preload of 2 N. Moreover, two sense electrodes made of copper wires were attached to the nanocomposite surface near the center of the sample with silver ink to minimize the contact resistance, keeping a distance between electrodes of 3 cm, as shown in Fig. 1c. In addition, compression specimens with $30 \times 20 \times 10\ mm^3$ dimensions were analyzed at a test rate of 1 mm/min and a preload of 1.5 N. Furthermore, two force electrodes were attached with silver ink to the upper and lower sample surfaces of the nanocomposites, as indicated in Fig. 1d. In these tests, it is important to note that samples were isolated from grips by using an adhesive layer at the ends of the specimens to avoid electrical interferences with the nanocomposite.

Tensile and compression monitoring tests allowed us to determine the Gauge Factor (GF), which is a critical parameter to determine sensor sensitivity and can be calculated as the normalized resistance change ($\Delta R/R_0$) divided by the applied strain (ε), as specified Eq. (1):

$$GF = \frac{\Delta R/R_0}{\varepsilon} = \frac{R - R_0}{R_0 \bullet \varepsilon} \quad (1)$$

To study the stable repeatability and life cycle of GNP/PEGDGE sensors, the same tensile and compression specimens were subjected to continuous strain cycling for 500 cycles at 1%, 2.5%, and 5% strain levels at 50 mm/min and 5 mm/min, respectively. Moreover, the electrical response of the optimized sensor under 20, 50, 90, 140, and 200 mm/min tensile frequencies was studied in 5 cycles. The transient response of the optimized sensor was evaluated by applying 1% and 5% strain levels at a strain rate of 500 mm/min and, after a few seconds, the recovery to the initial position at the same rate.

2.6. Proof of concept of wearable sensors

The sensor that achieved the best properties (combination of electrical conductivity, gauge factor, and cyclic robustness) was used for different proofs–of–concept for large and small movements. In this regard, the sensor with 8 wt% GNP manufactured was used for this purpose. First, three general tests were carried out to demonstrate that this sensor can detect several types of deformations: pressure, bending, and twisting. This sensor was cut with $50 \times 15 \times 3\ mm^3$ dimensions, as shown in Fig. 1e. Second, another test, this time detecting human breath was carried out by placing a sensor with $40 \times 4 \times 2\ mm^3$ dimensions in a conventional mask (FFP2) (Fig. 1f). In these tests, the location of the electrodes followed the same logic as that mentioned above.

Finally, several never seen trials of mask breath monitoring with this type of nanocomposite and by using IoT technology were performed using the four-wire electrical resistance method. Here, two electrodes named power electrodes with different polarity were connected to the edges of the nanocomposite with one of the ends and with the other two to a button plain battery which was glued to the surface of the FPP2 mask. In addition, the two other electrodes, named sense electrodes, were connected with one of their ends to two separated points of the nanocomposite and were positioned between the power electrodes, with the two other ends attached to the inputs of a LoRa emitter (MKRWAN1300). This configuration allowed measuring the change in resistance of the sensor material when it was either compressed or stretched as the mask was tightened or loosened due to the air intake or exhaled by the subject under study. The change in resistance of the sensor material was monitored by measuring the voltage drop between the sense electrodes.

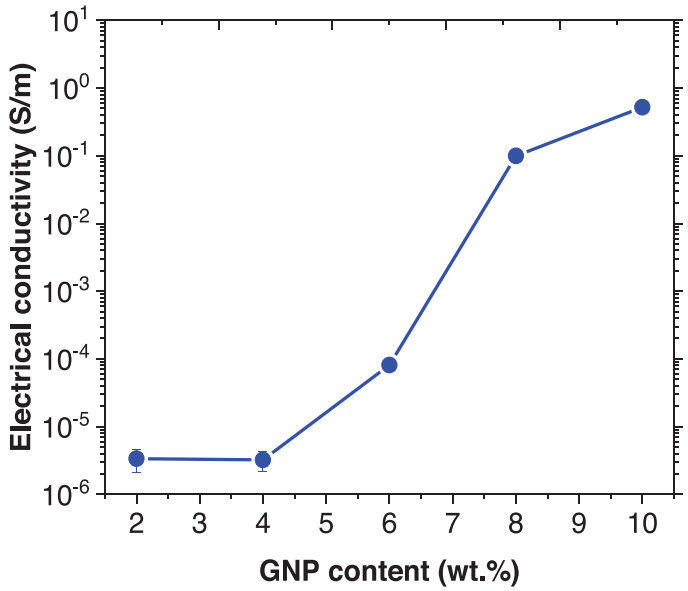

(a)

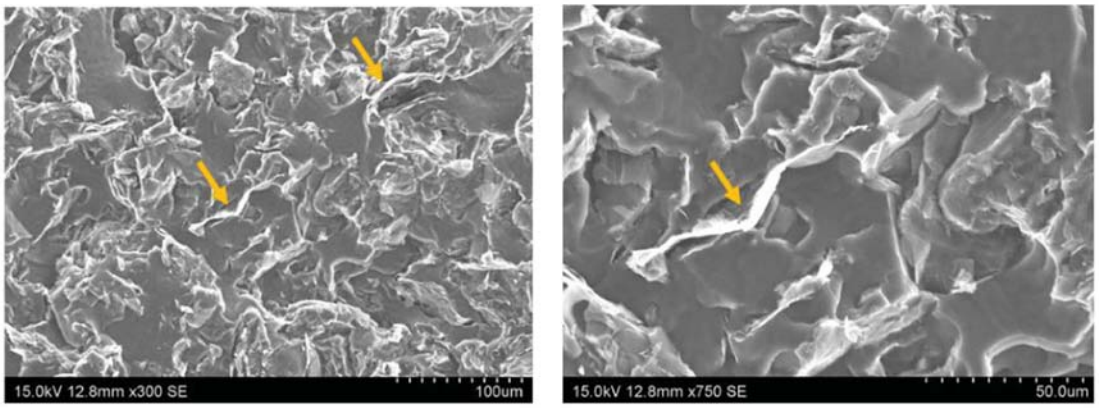

(b)

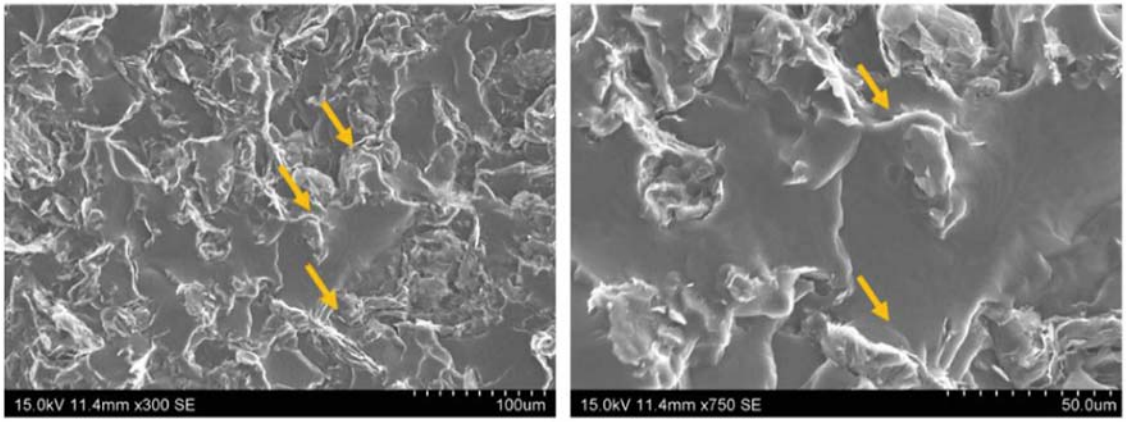

(c)

Fig. 2. (a) Electrical conductivity measurements of the GNP/PEGDGE nanocomposites under three–roll–mill technique. SEM images of cryofracture surfaces of (b) 2, (c) 4, (d) 6, (e) 8, and (f) 10 wt% GNP nanocomposites. The images on the left are at 300 magnifications, while those on the right are at 750 magnifications. Orange arrows indicate the presence of GNPs.

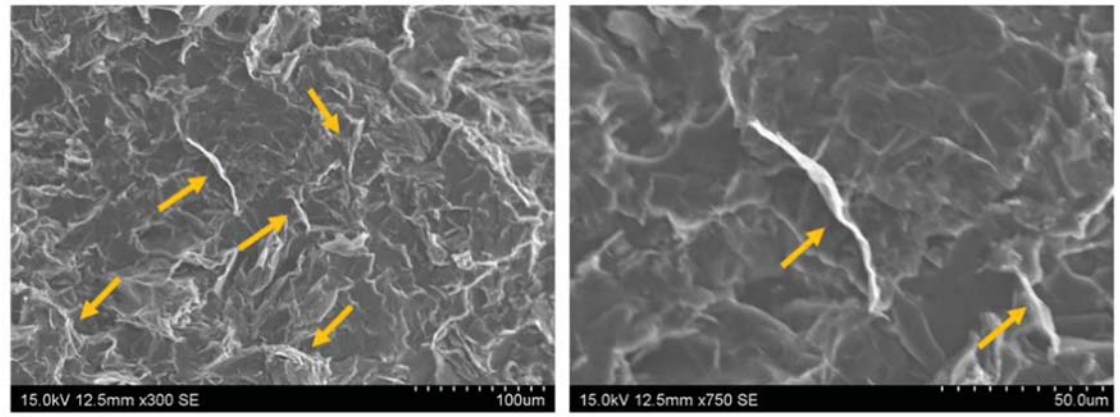

(d)

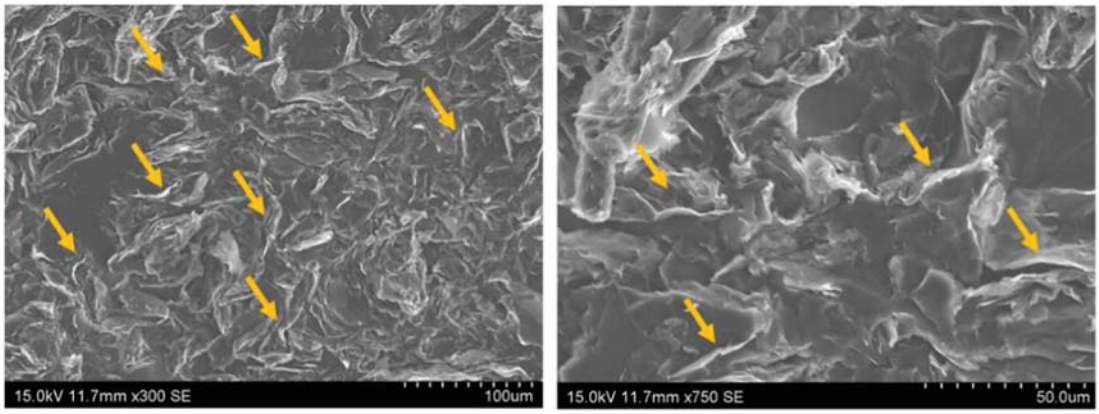

(e)

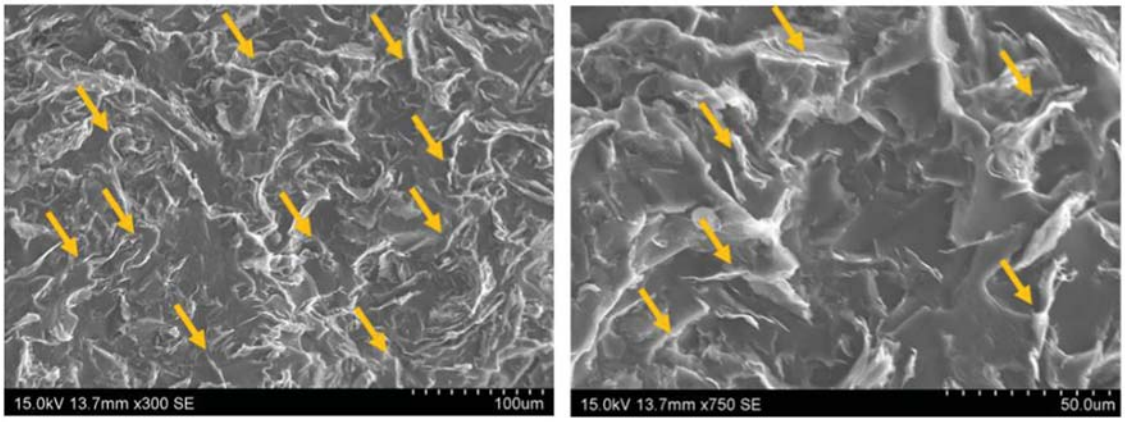

(f)

Fig. 2. (*continued*).

With the purpose of monitoring the subject breathing, MKRWAN1300 LoRa emitter received the voltage drop produced in the material by using the sensing electrodes connected to channel A0 and Ground. This LoRa emitter which was connected to the nanocomposite was kept in a bracelet that was attached to the forearm. Then, voltage signals were remotely sent to a gateway that could be located up to 20 km of distance from the emitter in interurban areas. Sixty-four bytes were sent every 7 s, and every byte represented a point of the voltage signal. The data frequency rate was 8.9 Hz from the subsequent one. Gateway used was a raspberry pi400 coupled to a RAK2245 Pi HAT LoRa concentrator and it was connected via Wi-Fi to the internet (Fig. 1g). Sensor and RAK were registered in The Things of Stack (TTS) IoT platform and all the information received by the RAK could be monitored with the software of Ubidots, which is connected to TTN with a parsed link.

To take advantage of the 1024 steps that MKRWAN uses to measure 5 V, this resolution was rescaled to 256 so that the whole 64 bytes of each data package were fully used. Information decoding is performed in the cloud, with a payload format that allowed transforming a vector of points with a frequency range of 120 ms into decimal values. Correlation

between Ubidots and the TTS is performed via HTTP (Hypertext Transfer Protocol) using the Webhook integration. In addition, Ubidots make use of another characteristic decoder that allows monitoring information given by TTS by its URL so that graphics of voltage vs time can be seen on the web.

With this smart mask, three experiments were performed by one of the authors. First, the subject began to breathe normally in a relaxed state. The second experiment consisted of mixing normal breathing and excited ones. In the last experiment, normal breathing is combined with walking.

3. Results and discussion

In this section, an analysis of the electrical response of GNP/PEGDGE nanocomposites is carried out by means of electrical conductivity measurements. Then, their strain-sensing capabilities are evaluated under tensile and compression conditions, to evaluate their electrical sensitivity to mechanical strain. Finally, a trial of GNP/PEGDGE as a wearable sensor is carried out, to test its applicability.

3.1. Electrical conductivity analysis

Fig. 2a shows the measured electrical conductivity of the GNP/PEGDGE nanocomposites for the different GNP contents manufactured.

It can be observed that the electrical conductivity increases with GNP content, as expected, due to the creation of more electrical pathways. More specifically, the percolation threshold is around 4 wt%. From 4–8 wt% a large increase of the electrical conductivity is observed, whereas at 10 wt% the electrical conductivity increase is quite lower, indicating that the electrical network saturation is being achieved. Moreover, electrical conductivity at 8 and 10 wt% is quite similar to the one obtained for similar systems using flexible resins [21], which is a good indicator of an efficient dispersion of the GNPs. GNP contents above 10 wt% were not tested because the significant enhancement of the electrical conductivity was not expected due to the massive interactions between nanoparticles, which could lead to a less efficient electrical network.

In this regard, good GNP dispersion was also established by the SEM cryofractures analysis. Homogeneous distribution of GNP in PEGDGE matrix was observed in Fig. 2b-f, where GNPs were highlighted with orange arrows. Here, there is no prevalence of large GNP aggregates. This good distribution is achieved regardless of GNP content. Moreover, it is shown that by increasing the GNP content, the number of nanoparticles observed in the cryofracture is higher, as expected. However, even in this case, there are no significant agglomerates in the nanocomposites, which explains the high efficiency of the electrical network generated and, thus, the high electrical conductivity values achieved.

Furthermore, the cryofracture surfaces shown in Fig. 2b-f denote that the higher the GNP content, the rougher or more fibrous the fracture surface. This fact is explained by the combination of two effects: the presence of a high number of nanoparticles that induces a crack–-bridging phenomenon, leading to a more tortuous crack propagation; and the fact that the lower physical force of union may cause stress concentrations around the GNPs, which is more prevalent at higher GNP contents.

3.2. Strain sensing tests

3.2.1. Quasi–static response

Fig. 3a shows the electromechanical curves of the GNP/PEGDGE sensors under tensile conditions. Here, it is important to point out that only the 8 and 10 wt% samples were tested as the electrical conductivity of the 2, 4, and 6 wt% samples were below the threshold of the monitoring device. It can be observed that the electrical resistance increases in a linear–exponential way with the applied strain. This is explained by the prevalence of the tunneling mechanisms between neighboring nanoparticles. This tunneling effect follows a linear–exponential way accordingly to the well–known Simmons formula [38]. In this regard, Fig. 3b summarizes the GF values calculated from the electromechanical curves as a function of the applied strain. It can be observed that the GF is higher for the 8 wt% samples, as expected, due to the higher tunneling distance between neighboring nanoparticles that induces a more pronounced exponential effect and, thus, a higher electrical sensitivity to mechanical strain. Moreover, the values of the GF are around 50–100 at low strain levels (1–2%) and around 1000–2500 at high strain levels (10%). These GF values are similar to those obtained for GNP-based sensors, which showed an ultrasensitive response [21,39–42], and are quite above those obtained for other nanoparticle–based sensors (rGO [43], CNT [44–46], AgNW [47,48], Gold [49]) and conventional metallic gauges (GF around 2–4) [50].

On the other hand, the electromechanical behavior under the compressive load of the GNP/PEGDGE sensors was also evaluated (Fig. 3c). Here, it can be observed that the electrical response is quite different from those observed at tensile conditions. First, a slight decrease in the electrical resistance is observed, whereas at higher strain levels the electrical resistance starts to increase. This behavior has been observed in other studies [51,52] and it is correlated to the different interactions that may take place between neighboring nanoparticles. At low strains, there is a decrease in the electrical resistance due to the prevalence of in–plane contacts, which induces a reduction of the tunneling distance between neighboring nanoparticles (Fig. 3d). However, at high strains, the out–of–plane contacts are much more prevalent and due to Poisson's effect, the out–of–plane interparticle distance is increased and, thus, the electrical resistance. Furthermore, Fig. 3e summarizes the GF values at compressive conditions. In this case, a reduction of the GF is observed when compared to tensile conditions. This reduction is explained by the previously commented combined effect of the in–plane and out–of–plane mechanisms. Moreover, the GF increases with decreasing the GNP content, as explained before, due to a higher prevalence of tunneling mechanisms by increasing the interparticle distance.

3.2.2. Cycling tests

The graphs of Fig. 4a-d show the electromechanical response of the GNP/PEGDGE sensors under cycling load for 500 tensile load cycles. Here, several can be stated. First, the change of the electrical resistance in a single cycle increase, as expected, with the applied strain and the decreasing GNP content due to the previously commented prevalence of tunneling mechanisms, as shown in Fig. 4a and b. It can be observed that the electrical resistance changes are even significant at low strain levels (1%), indicating the good applicability of the developed sensors for the detection of small movements. Second, it can be also noticed that the peak and baseline values of the electrical resistance slightly decrease with increasing the number of cycles. This effect can be correlated to the intrinsic viscoelastic behavior of the PEGDGE. In fact, a delayed response of the mechanical load can be observed with increasing the number of cycles. This delayed mechanical response induces, thus, a delayed electrical response that explains the changes in the peak and baseline values. In addition, these changes are more prevalent in the 10 wt% GNP samples as the delay in the mechanical response is also more pronounced (Fig. 4b and c). However, in any case, when comparing consecutive cycles, a robust electrical response can be found.

Fig. 4e-h summarizes the electromechanical response under cycling load in compressive conditions. Fig. 4e and f showed that the electrical resistance change in a single cycle is lower than in tensile conditions, as expected, due to the previously explained combined effect of the in–plane and out–of–plane mechanisms. Furthermore, it can be also noticed that the changes in the peak and baseline values throughout the test are more prevalent than in tensile conditions. This can be explained by the inherent irreversibility of the electrical network induced during the compression, which can be attributed to the presence of some irreversibility in the GNP network during load-unloading. Here, it is

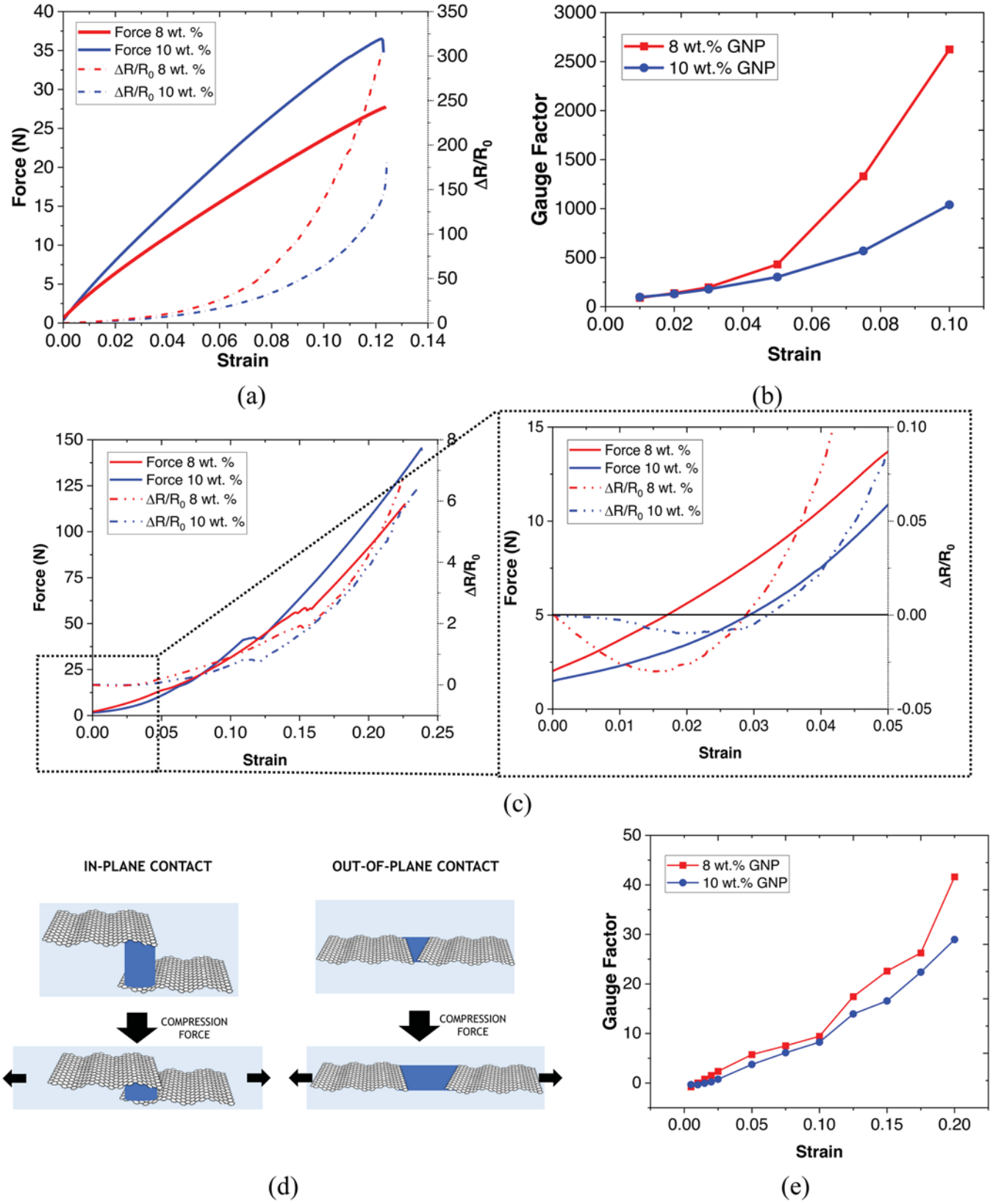

Fig. 3. (a) Electromechanical curves under tensile conditions, (b) GF as a function of applied strain during tensile test. (c) Electromechanical curves under compressive conditions, (d) schematics of in–plane and out–of–plane mechanisms during compression, and (e) GF as a function of applied strain during the compression test.

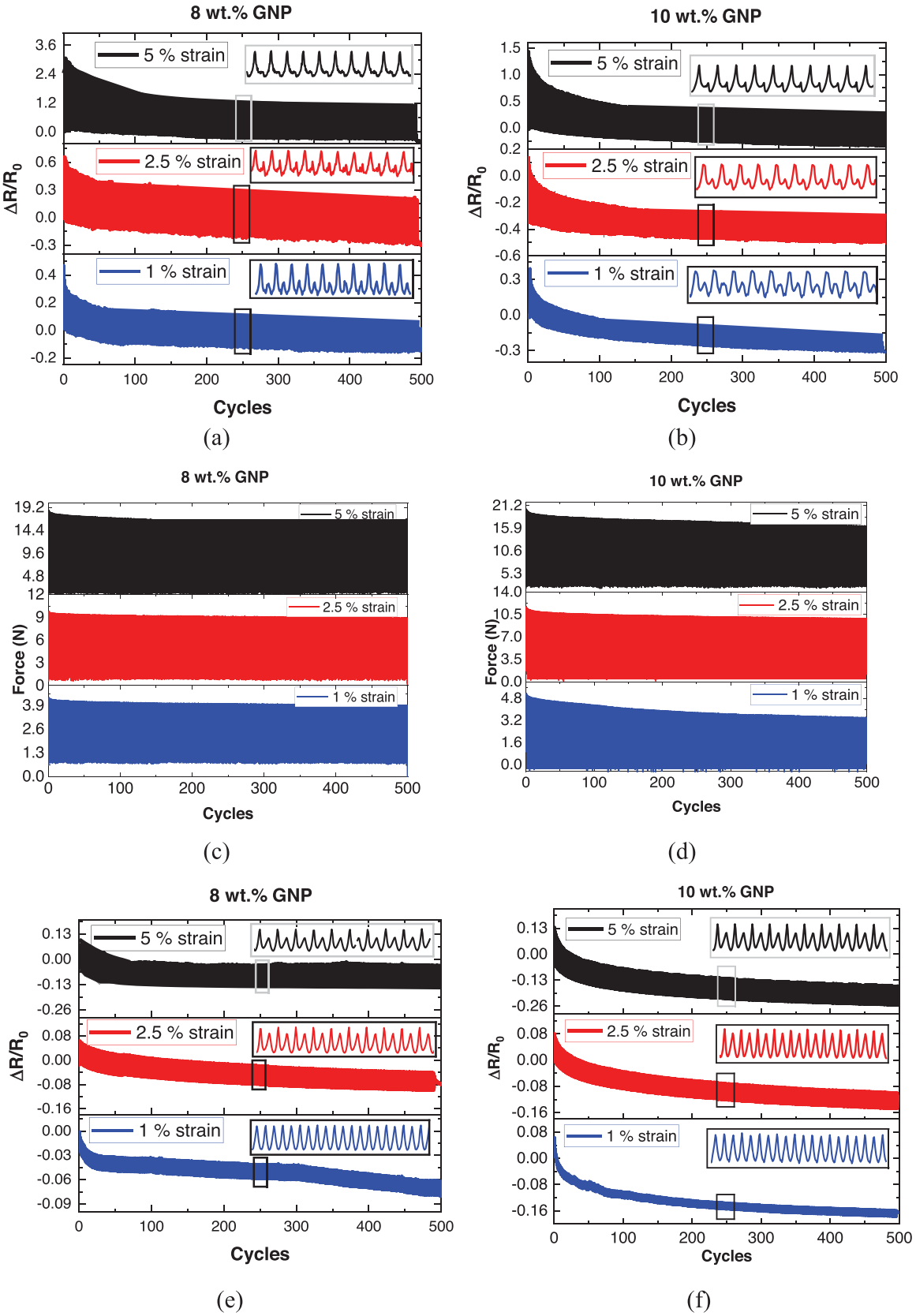

Fig. 4. : Electromechanical response under cycling load in tensile conditions for (a), (c) 8 wt% and (b), (d) 10 wt% GNP samples. Electromechanical response under cycling load in compressive conditions for (e), (g) 8 wt% and (f), (h) 10 wt% GNP samples. (i) Tensile cycling stability at different strain frequencies up to 5% strain level and (j) transient response up to 1% and 5% strain level of the 8 wt% GNP sensor.

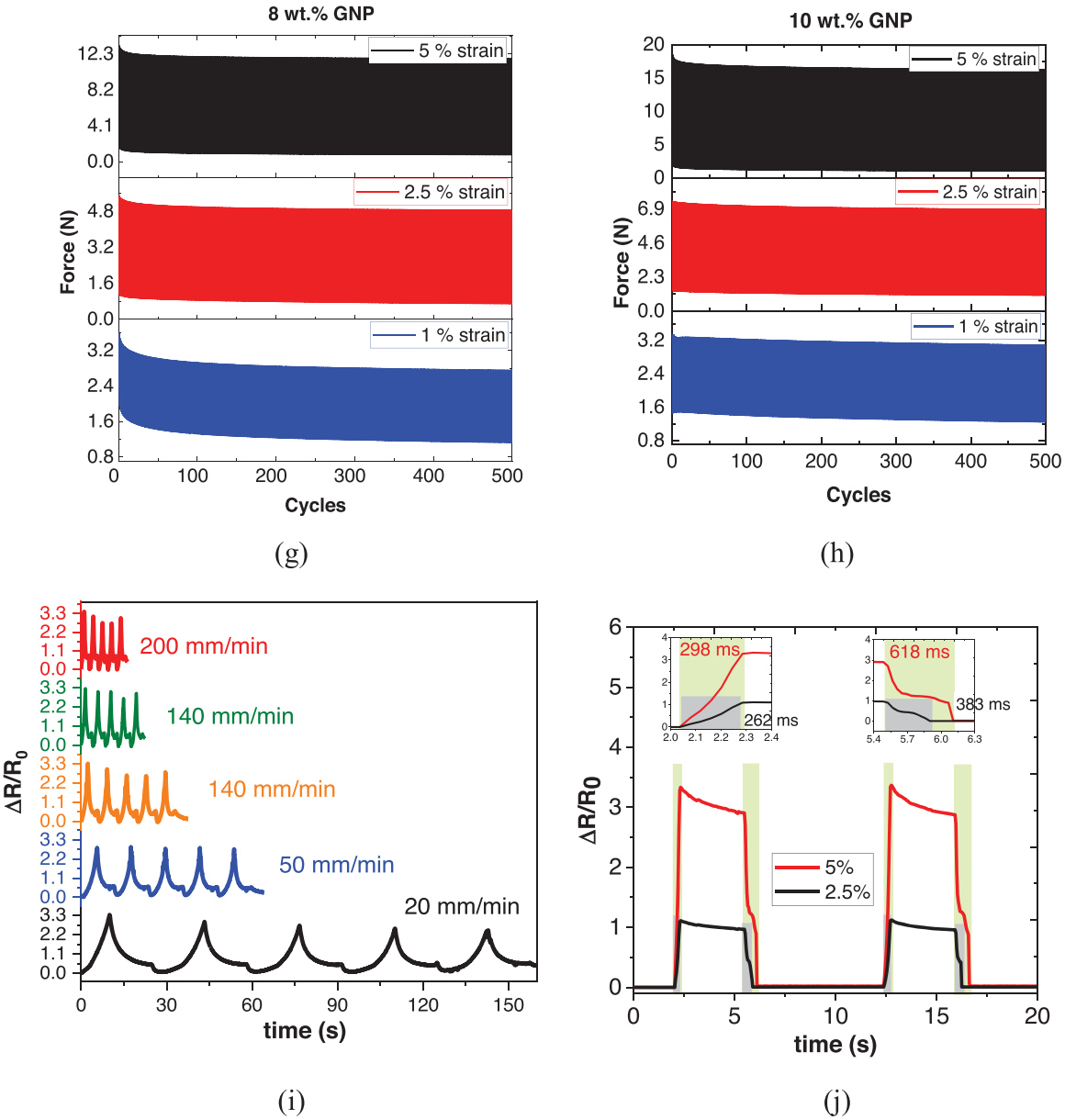

Fig. 4. (*continued*).

possible that the GNPs do not recover their initial position after the unloading, leading to the continuous creation and breakage of new electrical networks [53–55]. When increasing the number of cycles, however, the electrical response is more stable and the changes in the peak and baseline values are less pronounced.

It can be also observed that there is a delayed mechanical response (Fig. 4g and h), that contributes, as explained before, to the changes in the peak and baseline trends of the electrical response during the cycling test. However, again, the electrical response under consecutive cycles is found to be quite similar, indicating high robustness of the developed sensors.

Fig. 4i shows the electrical response of the 8 wt% GNP sensor under tensile dynamic load up to 5% strain with varying load frequency from 20 to 200 mm/min. Here, the electrical response indicates a similar sensitivity regardless of the frequency of the dynamic load, that is, good robustness. Finally, Fig. 4j presents the transient response in two cycles up to 1% and 5% strain levels. Both the response and recovery time are in the range of milliseconds (~300 and ~400–600 ms, respectively), which is in good agreement with the response and recovery times obtained for other similar sensors [56–58]. In addition, it can be observed a slight decrease when the applied strain is constant due to the inherent viscoelastic behavior of the matrix.

3.3. Proof–of–concept analysis

Several tests of GNP/PEGDGE sensors were carried out to prove their applicability as wearable strain sensors. The 8 wt% GNP samples were selected for these tests due to their higher electromechanical sensitivity in a wide range of strain levels, as observed before.

In this regard, Fig. 5 summarizes the results of these tests. It can be observed that the proposed sensors showed an ultrasensitive response to mechanical strain. More specifically, they were proven as pressure sensors (Fig. 5a). Here, it can be noticed that the electrical resistance increases when pressing the sensor and the variation is higher when increasing the pressing force (Video S1).

Supplementary material related to this article can be found online at doi:10.1016/j.sna.2023.114448.

A similar behavior is observed when subjecting the sensor to bending

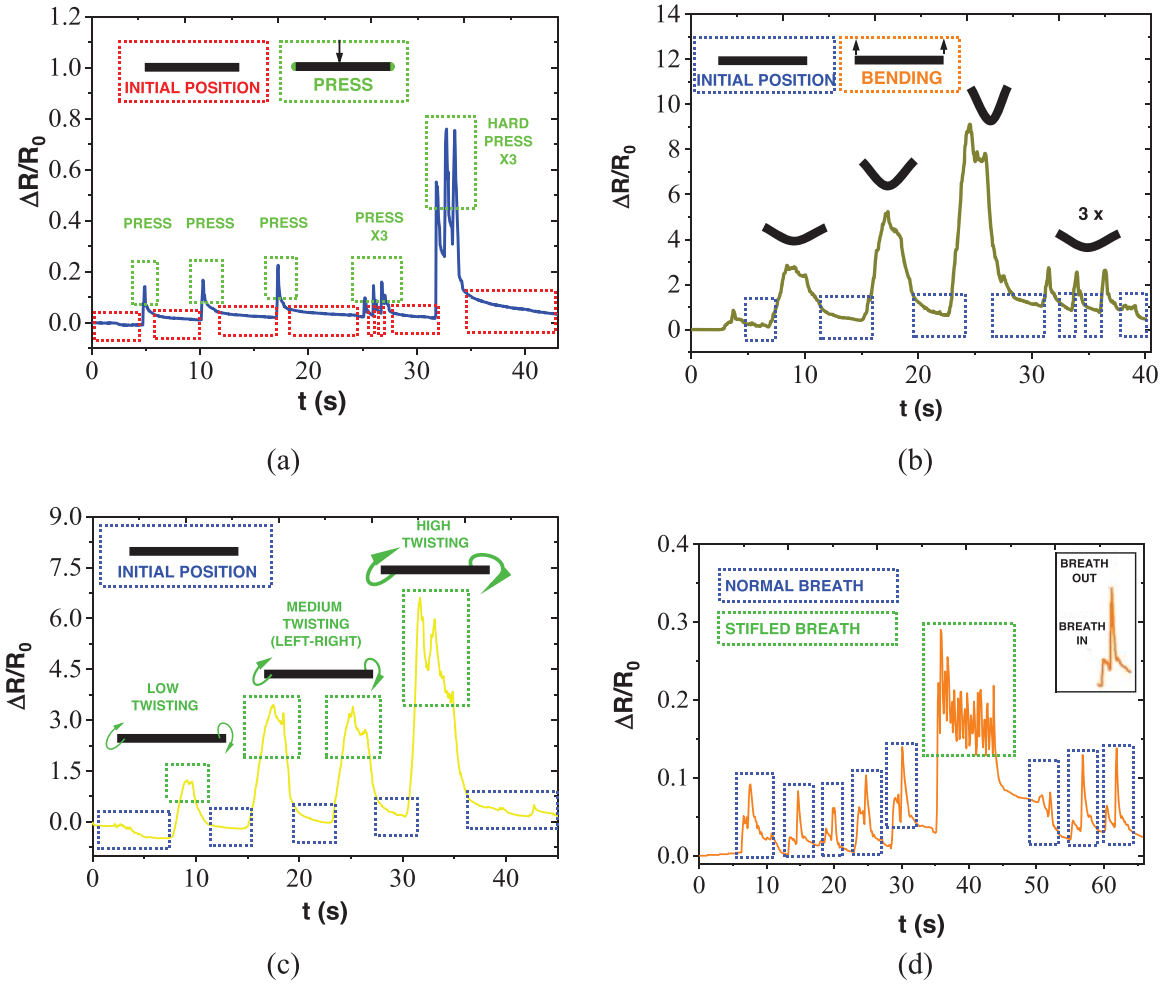

Fig. 5. : Electrical response of the optimized GNP/PEGDGE sensor (a) as a pressure sensor, under (b) bending or (c) twisting conditions and (d) breath detection in a FFP2 mask.

(Fig. 5b). Here, the electrical resistance changes accordingly to the bending degree (Video S2) and recovers the initial state during the stretching. Under twisting conditions (Fig. 5c) the behavior is quite similar, with a more prevalent increase of the electrical resistance when increasing the twisting angle of the sensor (Video S3). Therefore, these basic proof–of–concepts showed a high electrical sensitivity of the proposed sensors under low and high strain levels.

Supplementary material related to this article can be found online at doi:10.1016/j.sna.2023.114448.

Furthermore, Fig. 5d shows the resistance response of this sensor applied to a conventional mask for breath detection. It can be observed that the sensors are able to monitor both the breath–in and breath–out (Video S4). This can be explained because when the subject breathes, it induces a slight deformation of the mask, which is translated to a small strain on the sensor, leading to a significant change in its electrical response due to its proven ultra–high sensitivity. This capability for breathing monitoring was previously observed in another study by the authors using GNP/PDMS samples but directly applied to the neck. In this case, the application of these sensors over the mask surface would be much more practical.

Supplementary material related to this article can be found online at doi:10.1016/j.sna.2023.114448.

Regarding remotely monitoring a subject's breath with the nanocomposite attached to a mask, three different tests performed by the user in a relax mode, combining calm and exited states and breathing while walking gave proper results (Video S5, S6, and S7, respectively) and was in agreement with the resistance change signals measured directly with the multimeter. Fig. 6 shows the breath rhythm monitored in the IoT with Ubidots and TTS connected when voltage signals were transmitted remotely using LoRa communication protocol. Periodical pulses with frequency rates of 0.2 Hz and bandwidths of 1 Hz could be monitored properly on a big screen of a PC connected to the internet (Fig. 6a and c). A faster acquisition rate of 2 Hz could be observed when the subject was breathing in a more excited state (Fig. 6b). According to the results obtained, breath monitoring with LoRa communication protocol is possible despite its narrow bandwidth.

Supplementary material related to this article can be found online at doi:10.1016/j.sna.2023.114448.

Therefore, by analyzing this proof–of–concept it can be concluded that the developed material with remote tracking opens the possibility of monitoring the breath rhythm and other vital parameters in the screens of a hospital or client connected to a central server so that patients are monitored and controlled in real-time.

4. Conclusions

The electromechanical response and real–applicability with remote monitoring by using Internet of Things (IoT) technologies of ultrasensitive and stretchable sensors made of GNP–doped PEGDGE were investigated.

The analysis of strain monitoring response under both tensile and compression conditions of nanocomposites is studied in detail. According to quasi–static analysis, the values of the GF in tensile mode are around 50–100 at low strain levels (1–2%) and up to 1000–2500 at high

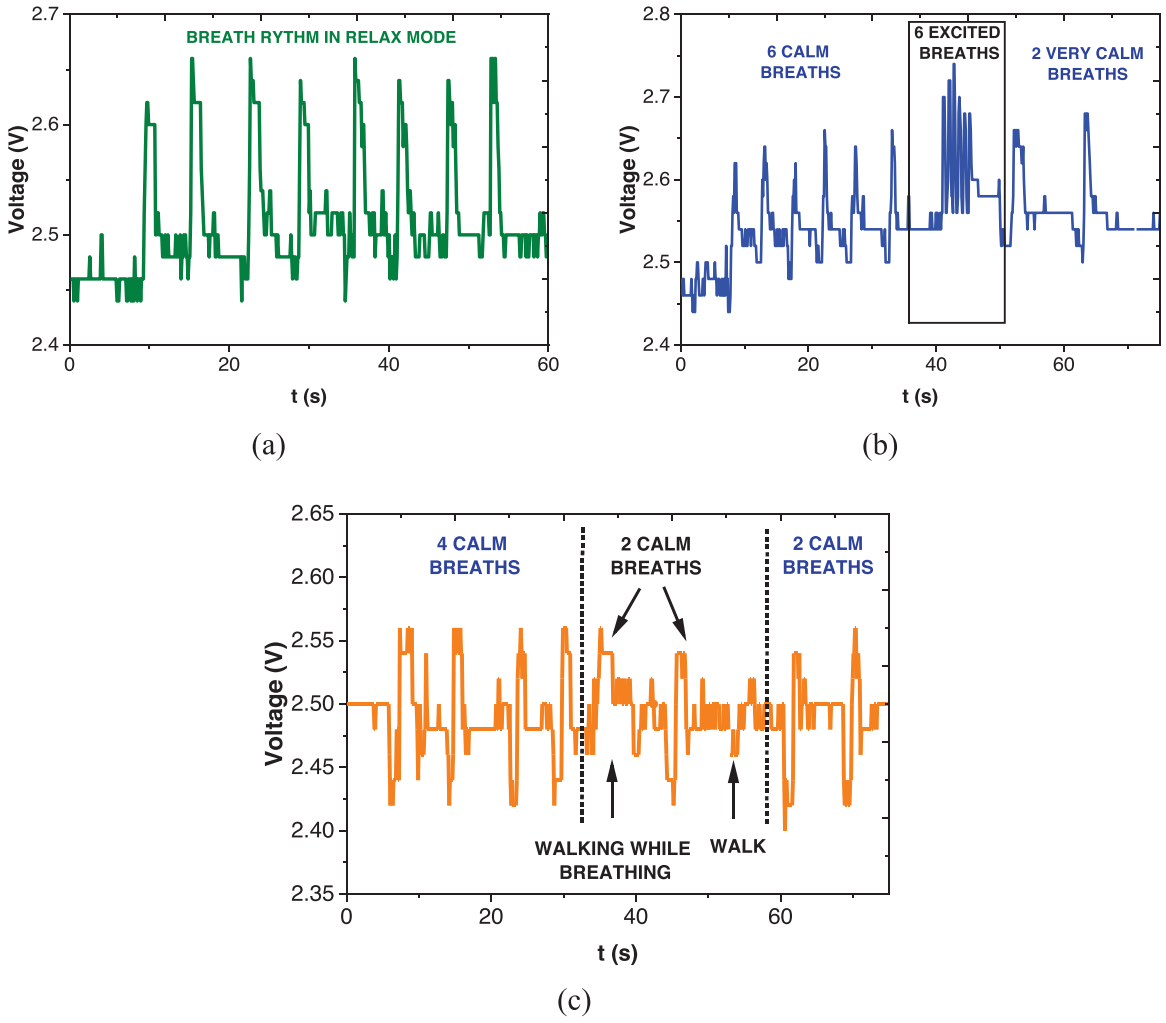

Fig. 6. : Remote mask breathing monitoring with LoRa/IoT technology (a) in a relaxed mode (b) in a calm and exited mode and, (c) in a calm mode while walking.

strain levels (10%), while the GF in compression mode is around 20 at low strain levels (5%) and 80 at high strain levels (20%). Regarding cycling tests, electromechanical responses under 500 tensile and compression load cycles up to 1%, 2.5%, and 5% strain levels prove their high stability and fast response.

The 8 wt% GNP nanocomposite was selected for the tests due to its higher electromechanical sensitivity. The general proofs–of–concepts for pressure, bending, and twisting demonstrate the ability of these sensors to detect various magnitudes and types of deformations. Finally, a trial of human breathing monitoring with the optimized sensor attached to the surface of the FFP2 mask is carried out. The subject's breathing rhythm (combining relaxed and excited modes while walking) is monitored remotely using the LoRa communication protocol on the Internet of Things and The Things of Stack.

Therefore, the easy–manufactured GNP/PEGDGE nanocomposites showed an outstanding potential and applicability in monitoring the human breath rhythm and other vital parameters in screens so that patients' health is known by doctors and relatives in real-time.

Supporting information

Video S1. Pressure sensing - Video S2. Bending sensing - Video S3. Twisting sensing – Video S4. Breathing monitoring – Video S5. Normal breath IoT – Video S6. Normal and stifled breath IoT - Video S7. Normal breath while walking IoT.

Declaration of Competing Interest

The authors declare that they have no known competing financial interests or personal relationships that could have appeared to influence the work reported in this paper.

Data Availability

Data will be made available on request.

Acknowledgements

This work was supported by the Agencia Estatal de Investigación of the Spanish Government [Project MULTIFUNC-EVs PID2019-107874RB-I00] and Comunidad de Madrid Government [Project ADITIMAT-CM (S2018/NMT-4411)]. This publication is partially funded through the project "MAMAP - Materials and models against pandemics" (REACT-EU resources of the Madrid Operational Program 2014–2020, in the action line of R+D+i projects in response to COVID-19). Project funded by the Community of Madrid and by the European Regional Development Fund of the European Union "A way to make Europe". Financed as part of the Union's response to the COVID-19 pandemic, through the agreement signed between the Community of Madrid (Regional Ministry of Education, Universities, Science, and Spokesperson) and the IMDEA Materials Foundation for the direct granting of a grant of 1.937.000 euros to fund research activities on SARS-COV 2 and

the COVID-19 disease funded with REACT-EU resources from the European Regional Development Fund.

References

[1] K.C. Kang, Y.H. Kim, J.Y. Pyun, K.K. Park, Feasibility study on multi-touch ultrasound large-panel touchscreen using guided lamb waves, Measurement 190 (2022), 110755, https://doi.org/10.1016/J.MEASUREMENT.2022.110755.

[2] O. Ahmed, X. Wang, M.V. Tran, M.Z. Ismadi, Advancements in fiber-reinforced polymer composite materials damage detection methods: towards achieving energy-efficient SHM systems, Compos. Part B Eng. 223 (2021), 109136, https://doi.org/10.1016/J.COMPOSITESB.2021.109136.

[3] S. Nag-Chowdhury, H. Bellégou, I. Pillin, M. Castro, P. Longrais, J.F. Feller, Crossed investigation of damage in composites with embedded quantum resistive strain sensors (sQRS), acoustic emission (AE) and digital image correlation (DIC), Compos. Sci. Technol. 160 (2018) 79–85, https://doi.org/10.1016/J.COMPSCITECH.2018.03.023.

[4] M.D. Crall, S.G. Laney, M.W. Keller, M.D. Crall, S.G. Laney, M.W. Keller, Multimodal damage detection in self-sensing fiber reinforced composites, Adv. Funct. Mater. 29 (2019) 1806634, https://doi.org/10.1002/ADFM.201806634.

[5] C. Tuloup, W. Harizi, Z. Aboura, Y. Meyer, K. Khellil, R. Lachat, On the use of in-situ piezoelectric sensors for the manufacturing and structural health monitoring of polymer-matrix composites: a literature review, Compos. Struct. 215 (2019) 127–149, https://doi.org/10.1016/J.COMPSTRUCT.2019.02.046.

[6] P. Govindaraj, A. Sokolova, N. Salim, S. Juodkazis, F.K. Fuss, B. Fox, N. Hameed, Distribution states of graphene in polymer nanocomposites: a review, Compos. Part B Eng. 226 (2021), 109353, https://doi.org/10.1016/J.COMPOSITESB.2021.109353.

[7] Y. Lu, M.C. Biswas, Z. Guo, J.W. Jeon, E.K. Wujcik, Recent developments in bio-monitoring via advanced polymer nanocomposite-based wearable strain sensors, Biosens. Bioelectron. 123 (2019) 167–177, https://doi.org/10.1016/J.BIOS.2018.08.037.

[8] M. Amjadi, K.-U. Kyung, I. Park, M. Sitti, M. Amjadi, M. Sitti, K. Kyung, I. Park, Stretchable, skin-mountable, and wearable strain sensors and their potential applications: a review, Adv. Funct. Mater. 26 (2016) 1678–1698, https://doi.org/10.1002/ADFM.201504755.

[9] H. Souri, H. Banerjee, A. Jusufi, N. Radacsi, A.A. Stokes, I. Park, M. Sitti, M. Amjadi, Wearable and stretchable strain sensors: materials, sensing mechanisms, and applications, Adv. Intell. Syst. 2 (2020) 2000039, https://doi.org/10.1002/AISY.202000039.

[10] M. Li, S. Chen, B. Fan, B. Wu, X. Guo, Printed flexible strain sensor array for bendable interactive surface, Adv. Funct. Mater. 30 (2020) 2003214, https://doi.org/10.1002/ADFM.202003214.

[11] A. del Bosque, X.F. Sánchez-Romate, M. Sánchez, A. Ureña, Flexible wearable sensors based in carbon nanotubes reinforced poly(ethylene glycol) diglycidyl ether (PEGDGE): analysis of strain sensitivity and proof of concept, Chemosensors 9 (2021) 158, https://doi.org/10.3390/chemosensors9070158.

[12] N.T. Selvan, S.B. Eshwaran, A. Das, K.W. Stöckelhuber, S. Wießner, P. Pötschke, G. B. Nando, A.I. Chervanyov, G. Heinrich, Piezoresistive natural rubber-multiwall carbon nanotube nanocomposite for sensor applications, Sens. Actuators A Phys. 239 (2016) 102–113, https://doi.org/10.1016/J.SNA.2016.01.004.

[13] S. Baloda, Z.A. Ansari, S. Singh, N. Gupta, Development and analysis of graphene nanoplatelets (GNPs)-based flexible strain sensor for health monitoring applications, IEEE Sens. J. 20 (2020) 13302–13309, https://doi.org/10.1109/JSEN.2020.3004574.

[14] G. Shi, S.E. Lowe, A.J.T. Teo, T.K. Dinh, S.H. Tan, J. Qin, Y. Zhang, Y.L. Zhong, H. Zhao, A versatile PDMS submicrobead/graphene oxide nanocomposite ink for the direct ink writing of wearable micron-scale tactile sensors, Appl. Mater. Today 16 (2019) 482–492, https://doi.org/10.1016/J.APMT.2019.06.016.

[15] J. Wu, Z. Ma, Z. Hao, J.T. Zhang, P. Sun, M. Zhang, Y. Liu, Y. Cheng, Y. Li, B. Zhong, T. Zhang, L. Xia, W. Yao, X. Huang, H. Wang, H. Liu, F. Yan, C.E. Hsu, G. Xing, Sheath-core fiber strain sensors driven by in-situ crack and elastic effects in graphite nanoplate composites, ACS Appl. Nano Mater. 2 (2019) 750–759, https://pubs.acs.org/doi/abs/10.1021/acsanm.8b01926.

[16] P. Song, G. Wang, Y. Zhang, Preparation and performance of graphene/carbon black silicone rubber composites used for highly sensitive and flexible strain sensors, Sens. Actuators A Phys. 323 (2021), 112659, https://doi.org/10.1016/J.SNA.2021.112659.

[17] K. Ke, V. Solouki Bonab, D. Yuan, I. Manas-Zloczower, Piezoresistive thermoplastic polyurethane nanocomposites with carbon nanostructures, Carbon N. Y 139 (2018) 52–58, https://doi.org/10.1016/J.CARBON.2018.06.037.

[18] Q. Liu, J. Chen, Y. Li, G. Shi, High-performance strain sensors with fish-scale-like graphene-sensing layers for full-range detection of human motions, ACS Nano. 10 (2016) 7901–7906, https://pubs.acs.org/doi/abs/10.1021/acsnano.6b03813.

[19] P. Cataldi, L. Ceseracciu, A. Athanassiou, I.S. Bayer, Healable cotton-graphene nanocomposite conductor for wearable electronics, ACS Appl. Mater. Interfaces 9 (2017) 13825–13830, https://doi.org/10.1021/ACSAMI.7B02326/.

[20] A. Del Bosque, X.F. Sánchez-Romate, M. Sánchez, A. Ureña, Wearable sensors based on graphene nanoplatelets reinforced polydimethylsiloxane for human motion monitoring: analysis of crack propagation and cycling load monitoring, Chemosensors 10 (2022) 75, https://doi.org/10.3390/chemosensors10020075.

[21] A. del Bosque, X.F. Sánchez-Romate, M. Sánchez, A. Ureña, Ultrasensitive and highly stretchable sensors for human motion monitoring made of graphene reinforced polydimethylsiloxane: electromechanical and complex impedance sensing performance, Carbon 192 (2022) 234–248, https://doi.org/10.1016/j.carbon.2022.02.043.

[22] H. Hu, Y. Ma, J. Yue, F. Zhang, Porous GNP/PDMS composites with significantly reduced percolation threshold of conductive filler for stretchable strain sensors, Compos. Commun. 29 (2022), 101033, https://doi.org/10.1016/J.COCO.2021.101033.

[23] Y. Zheng, Y. Li, Z. Li, Y. Wang, K. Dai, G. Zheng, C. Liu, C. Shen, The effect of filler dimensionality on the electromechanical performance of polydimethylsiloxane based conductive nanocomposites for flexible strain sensors, Compos. Sci. Technol. C. (2017) 64–73, https://doi.org/10.1016/J.COMPSCITECH.2016.12.014.

[24] Y.A. Samad, Y. Li, S.M. Alhassan, K. Liao, Novel graphene foam composite with adjustable sensitivity for sensor applications, ACS Appl. Mater. Interfaces 7 (2015) 9196–9202, https://doi.org/10.1021/ACSAMI.5B01608.

[25] Y.A. Samad, Y. Li, A. Schiffer, S.M. Alhassan, K. Liao, Graphene Foam Developed with a Novel Two-Step Technique for Low and High Strains and Pressure-Sensing Applications, (2015). https://doi.org/10.1002/smll.201403532.

[26] J. Li, S. Zhao, X. Zeng, W. Huang, Z. Gong, G. Zhang, R. Sun, C.P. Wong, Highly stretchable and sensitive strain sensor based on facilely prepared three-dimensional graphene foam composite, ACS Appl. Mater. Interfaces 8 (2016) 18954–18961, https://doi.org/10.1021/ACSAMI.6B05088.

[27] J. Hyysalo, S. Dasanayake, J. Hannu, C. Schuss, M. Rajanen, T. Leppänen, D. Doermann, J. Sauvola, Smart mask – wearable IoT solution for improved protection and personal health, Internet Things 18 (2022), 100511, https://doi.org/10.1016/J.IOT.2022.100511.

[28] S. Tian, W. Yang, J.M. Le Grange, P. Wang, W. Huang, Z. Ye, Smart healthcare: making medical care more intelligent, Glob. Heal. J. 3 (2019) 62–65, https://doi.org/10.1016/J.GLOHJ.2019.07.001.

[29] M. Haghi Kashani, M. Madanipour, M. Nikravan, P. Asghari, E. Mahdipour, A systematic review of IoT in healthcare: applications, techniques, and trends, J. Netw. Comput. Appl. 192 (2021), 103164, https://doi.org/10.1016/J.JNCA.2021.103164.

[30] D.-R. Izdrui, M.G. Hagan, O. Geman, O. Postolache, R. Alexandre, Smart sensing systems for in-home health status and emotional well-being monitoring during COVID-19, Biomed. Eng. Tools Manag. Patients COVID 19 (2021) 173–186, https://doi.org/10.1016/B978-0-12-824473-9.00003-3.

[31] S. Xu, Z. Fan, S. Yang, Y. Zhao, L. Pan, Flexible, self-powered and multi-functional strain sensors comprising a hybrid of carbon nanocoils and conducting polymers, Chem. Eng. J. 404 (2021), 126064, https://doi.org/10.1016/J.CEJ.2020.126064.

[32] Y. Lu, Industry 4.0: A survey on technologies, applications and open research issues, J. Ind. Inf. Integr. 6 (2017) 1–10, https://doi.org/10.1016/J.JII.2017.04.005.

[33] L.K. Ketshabetswe, A.M. Zungeru, M. Mangwala, J.M. Chuma, B. Sigweni, Communication protocols for wireless sensor networks: a survey and comparison, Heliyon 5 (2019), e01591, https://doi.org/10.1016/J.HELIYON.2019.E01591.

[34] A. Khalifeh, K.A. Aldahdouh, K.A. Darabkh, W. Al-Sit, A survey of 5G emerging wireless technologies featuring LoRaWAN, Sigfox, NB-IoT and LTE-M, Int, Conf. Wirel. Commun. Signal Process. Networking, WiSPNET (2019) 561–566, https://doi.org/10.1109/WISPNET45539.2019.9032817.

[35] N. Naik, LPWAN technologies for IoT systems: choice between ultra narrow band and spread spectrum, 4th IEEE Int. Symp. Syst. Eng. ISSE 2018 - Proc. (2018) 1–8. doi: 10.1109/SYSENG.2018.8544414.

[36] J. Chen, K. Hu, Q. Wang, Y. Sun, Z. Shi, S. He, Narrowband internet of things: implementations and applications, IEEE Internet Things J. 4 (2017) 2309–2314, https://doi.org/10.1109/JIOT.2017.2764475.

[37] X.F. Sánchez-Romate, V. Saiz, A. Jiménez-Suárez, M. Campo, A. Ureña, The role of graphene interactions and geometry on thermal and electrical properties of epoxy nanocomposites: a theoretical to experimental approach, Polym. Test. 90 (2020), 106638, https://doi.org/10.1016/J.POLYMERTESTING.2020.106638.

[38] J.G. Simmons, Generalized formula for the electric tunnel effect between similar electrodes separated by a thin insulating film, J. Appl. Phys. 34 (2004) 1793, https://doi.org/10.1063/1.1702682.

[39] A. del Bosque, X.F. Sánchez-Romate, D. Calvo, M. Sánchez, A. Ureña, Mechanical and sensing performance under hydrothermal ageing of wearable sensors made of polydimethylsiloxane with graphitic nanofillers, Polym. Degrad. Stab. 209 (2023), 110278, https://doi.org/10.1016/J.POLYMDEGRADSTAB.2023.110278.

[40] A. del Bosque, X.F. Sánchez-Romate, A. Gómez, M. Sánchez, A. Ureña, Highly stretchable strain sensors based on graphene nanoplatelet-doped ecoflex for biomedical purposes, Sens. Actuators A Phys. 353 (2023), 114249, https://doi.org/10.1016/J.SNA.2023.114249.

[41] A. Mehmood, N.M. Mubarak, M. Khalid, R. Walvekar, E.C. Abdullah, M.T. H. Siddiqui, H.A. Baloch, S. Nizamuddin, S. Mazari, Graphene based nanomaterials for strain sensor application—a review, J. Environ. Chem. Eng. 8 (2020), 103743, https://doi.org/10.1016/J.JECE.2020.103743.

[42] K. Huang, S. Dong, J. Yang, J. Yan, Y. Xue, X. You, J. Hu, L. Gao, X. Zhang, Y. Ding, Three-dimensional printing of a tunable graphene-based elastomer for strain sensors with ultrahigh sensitivity, Carbon N. Y 143 (2019) 63–72, https://doi.org/10.1016/J.CARBON.2018.11.008.

[43] X. Xia, G.J. Weng, J. Zhang, Y. Li, The effect of temperature and graphene concentration on the electrical conductivity and dielectric permittivity of graphene–polymer nanocomposites, Acta Mech. 231 (2020) 1305–1320, https://doi.org/10.1007/S00707-019-02588-4/FIGURES/11.

[44] A. Del Bosque, X.F. Sánchez-Romate, M. Sánchez, A. Ureña, Easy-scalable flexible sensors made of carbon nanotube-doped polydimethylsiloxane: analysis of manufacturing conditions and proof of concept, Sensors 22 (2022) 5147, https://doi.org/10.3390/S22145147.

[45] Y. Wang, S. Wang, M. Li, Y. Gu, Z. Zhang, Piezoresistive response of carbon nanotube composite film under laterally compressive strain, Sens. Actuators A Phys. 273 (2018) 140–146, https://doi.org/10.1016/J.SNA.2018.02.032.
[46] D.H. Joo, M.S. Kang, S.J. Park, S.A. Yu, W.T. Park, Fabrication method of flexible strain sensors with CNTs and solvents, Sens. Actuators A Phys. 345 (2022), 113775, https://doi.org/10.1016/J.SNA.2022.113775.
[47] R. Madhavan, Flexible and stretchable strain sensors fabricated by inkjet printing of silver nanowire-ecoflex composites, J. Mater. Sci. Mater. Electron. 33 (2022) 3465–3484, https://doi.org/10.1007/S10854-021-07540-8.
[48] Y. Yang, S. Duan, W. Xiao, H. Zhao, Silver nanowire-based stretchable strain sensors with hierarchical wrinkled structures, Sens. Actuators A Phys. 343 (2022), 113653, https://doi.org/10.1016/J.SNA.2022.113653.
[49] M. Duyen Ho, Y. Ling, L. Wei Yap, Y. Wang, D. Dong, Y. Zhao, W. Cheng, M.D. Ho, Y. Ling, L.W. Yap, Y. Wang, D. Dong, Y. Zhao, W. Cheng, Percolating network of ultrathin gold nanowires and silver nanowires toward "invisible" wearable sensors for detecting emotional expression and apexcardiogram, Adv. Funct. Mater. 27 (2017) 1700845, https://doi.org/10.1002/ADFM.201700845.
[50] X.F. Sánchez-Romate, J. Artigas, A. Jiménez-Suárez, M. Sánchez, A. Güemes, A. Ureña, Critical parameters of carbon nanotube reinforced composites for structural health monitoring applications: empirical results versus theoretical predictions, Compos. Sci. Technol. 171 (2019) 44–53, https://doi.org/10.1016/J.COMPSCITECH.2018.12.010.
[51] X.F. Sánchez-Romate, R. Moriche, A. Jiménez-Suárez, M. Sánchez, S.G. Prolongo, A. Ureña, Sensitive response of GNP/epoxy coatings as strain sensors: analysis of tensile-compressive and reversible cyclic behavior, Smart Mater. Struct. 29 (2020), 065012, https://doi.org/10.1088/1361-665X/AB8316.
[52] R. Moriche, M. Sánchez, A. Jiménez-Suárez, S.G. Prolongo, A. Ureña, Strain monitoring mechanisms of sensors based on the addition of graphene nanoplatelets into an epoxy matrix, Compos. Sci. Technol. 123 (2016) 65–70, https://doi.org/10.1016/J.COMPSCITECH.2015.12.002.
[53] X. Li, Y. Ren, X. Wang, S. Shao, H. Li, L. Wu, X. Liu, J. Zhao, Universal Method for High-Efficiency Immobilization of Semiconducting Carbon Nanotubes toward Fully Printed Paper-Based Electronics, Adv. Electron. Mater. 7 (2021) 2001025, https://doi.org/10.1002/AELM.202001025.
[54] S. Han, X. Zhang, P. Wang, J. Dai, G. Guo, Q. Meng, J. Ma, Mechanically robust, highly sensitive and superior cycling performance nanocomposite strain sensors using 3-nm thick graphene platelets, Polym. Test. 98 (2021), 107178, https://doi.org/10.1016/J.POLYMERTESTING.2021.107178.
[55] X. Zhang, D. Xiang, Y. Wu, E. Harkin-Jones, J. Shen, Y. Ye, W. Tan, J. Wang, P. Wang, C. Zhao, Y. Li, High-performance flexible strain sensors based on biaxially stretched conductive polymer composites with carbon nanotubes immobilized on reduced graphene oxide, Compos. Part A Appl. Sci. Manuf. 151 (2021), 106665, https://doi.org/10.1016/J.COMPOSITESA.2021.106665.
[56] C.M. Boutry, Y. Kaizawa, B.C. Schroeder, A. Chortos, A. Legrand, Z. Wang, J. Chang, P. Fox, Z. Bao, A stretchable and biodegradable strain and pressure sensor for orthopaedic application, 2018 15, Nat. Electron. 1 (2018) 314–321, https://doi.org/10.1038/s41928-018-0071-7.
[57] W. Bin Zhu, S.S. Xue, H. Zhang, Y.Y. Wang, P. Huang, Z.H. Tang, Y.Q. Li, S.Y. Fu, Direct ink writing of a graphene/CNT/silicone composite strain sensor with a near-zero temperature coefficient of resistance, J. Mater. Chem. C. 10 (2022) 8226–8233, https://doi.org/10.1039/D2TC00918H.
[58] W. Zhang, X. Zhang, W. Zhao, X. Wang, High-sensitivity composite dual-network hydrogel strain sensor and its application in intelligent recognition and motion monitoring, ACS Appl. Polym. Mater. (2022), https://doi.org/10.1021/ACSAPM.2C02215.

Dr. Antonio del Bosque (Ph.D. in Materials Science) started his research in the Materials Science and Engineering Area at Rey Juan Carlos University in 2019. His research activity is focused on the development of structural composites and high-performance nanocomposites for sensing (human motion monitoring, structural health monitoring, self-sensing…). Moreover, he has a vast experience in the characterization of energy storage devices.

Dr. Xoan Xosé F. Sánchez-Romate (Ph.D. in Aerospace Engineering) is an associate professor of Materials Science and Engineering Area at Rey Juan Carlos University since 2015. His research activity is focused on the application of carbon nanoparticles to develop multifunctional composite structures and polymers with self-sensing properties.

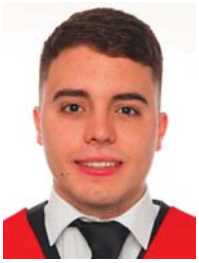

Mr. David Patrizi García is an Industrial Engineer with a degree in Electronics and Automation graduated from the Polytechnic University of Madrid. He has just started his research activity with a fellowship at IMDEA Materials Institute.

Dr. José Sánchez del Río Sáez (Ph.D in Materials Physics from Madrid Autonomous University and IMM-CSIC in 2007) was specialized as a postdoc at IEM-CSIC in nuclear instrumentation, biometrics and testing EEE components for space applications. Currently, he works as visiting scientist in research group of high performance polymer nanocomposites of IMDEA Materials Institute and at ICAI School of Engineering. He published more than 50 papers in peer-reviewed international journals and had over 10 international/national patents. He is lecturer in Physics and Electronics in Technical School of Industrial Engineering and Design (ETSIDI) of Polytechnic University of Madrid (UPM).

Prof. Dr. De-Yi Wang got his PhD degree in Polymer Chemistry and Physics at Sichuan University in China in 2007. Later on, he joined Leibniz-Institut für Polymerforschung Dresden E. V. Germany as Alexander Humboldt Fellow in 2010. He currently is the Senior Researcher at IMDEA Materials Institute in Madrid and leads the research group of High Performance Polymer Nanocomposites. In 2016, he elected as the Fellow of Royal Society of Chemistry, UK. His research interests mainly focus on new generation fire retardant materials, fire-safe energy materials, smart sensors and polymer nanocomposites, etc.

Prof. Dr. María Sánchez (Ph.D. in Materials Science) is a full professor in the Materials Science and Engineering Area at Rey Juan Carlos University since 2022. Her research activity is focused on the application of carbon nanoparticles to the improvement of properties and the development of new functionalities in polymers and polymeric matrix composite materials. Moreover, she develops brazing of refractory materials for their application in the future nuclear fusion reactor DEMO.

Prof. Dr. Alejandro Ureña (Ph.D. in Chemical Sciences and European Welding Engineer) is a full professor in the Materials Science and Engineering Area at Rey Juan Carlos University since 2002. His research activity follows two main lines: The application of nanotechnology to the improvement of properties and the development of new functionalities in polymers and polymeric matrix composite materials; and the brazing of refractory materials for their application in the nuclear fusion reactor DEMO.